*Indian J. Met. Hydrol. Geophys.* (1978), 29, 1 & 2, 308-313

551.553.21 : 551.509.313 : 551.511.3

# *A numerical study of the locally unstable barotropic easterly jet*

J. B. TUPAZ

*Naval Environmental Prediction Research Facility*
*Monterey, California*

and

R. T. WILLIAMS & C.-P. CHANG

*Department of Meteorology, Naval Postgraduate School*
*Monterey, California*

ABSTRACT. The structure and behaviour of barotropically unstable disturbances in the vicinity of the upper tropospheric easterly jet during the summer monsoon is studied numerically with a linearized barotropic vorticity equation on an equatorial $\beta$-plane. The easterly jet is approximated by a Bickley jet with a slow zonal variation, and the numerical results are compared with those of a simple theoretical model using the local phase speed and growth rate concepts. In the unstable region the resultant structure of the waves causes a spatial growth greater than that predicted by the local growth rates deduced from a parallel flow model. In the stable region the structure leads to strong dynamic damping. The implications of the removal of planetary scale kinetic energy by the unstable short waves are also discussed.

## 1. Introduction

In the northern hemisphere summer a strong easterly jet exists south of the Tibetan high at the 200 mb level (Krishnamurti and Rogers 1970). Synoptic-scale moving disturbances occur at the level of the jet, and it appears that these disturbances arise from barotropic instability of the basic flow. The jet contains regions of large vorticity gradient where the necessary condition for barotropic instability is sometimes satisfied locally. If the observed disturbances were the result of barotropic instability, they would extract energy from the mean flow and the long waves, since these waves combine with the mean flow to give the large vorticity gradient south of the Tibetan high. Kanamitsu *et al.* (1972) have in fact showed that wave numbers 6-8 in the wind spectrum in the region between 15°S and 15°N receive energy through barotropic interaction with the zonal mean flow and zonal wave number 1.

In order to obtain a better understanding of these upper tropospheric waves we study the behaviour of barotropic waves in a region of variable mean wind. We are especially interested in the situation where waves move into or out of barotropically unstable regions. Colton (1973) used a semi-spectral numerical model to study the barotropic interaction between disturbances and the mean flow. His long waves were forced with a specified divergence field following the diagnostic model of Holton and Colton (1972). He observed disturbances forming in the easterly jet over the Indian Ocean, and as the disturbances moved out of this region they tended to dissipate.

In this study we employ the linearized barotropic vorticity equation in a rectangular domain. The mean zonal wind is an easterly hyperbolic-squared jet and the mean meridional wind is derived in such a way that the mean flow is non-divergent. Periodic forcing is introduced on the eastern boundary and a radiation condition is applied at the western boundary. As the waves move through the region they grow or decay in relation to the local stability properties of the mean flow, whereas at each point the fields vary periodically.

## 2. Basic equations

The streamfunction for the non-divergent vorticity equation is broken up as follows :

$$\psi(x, y, t) = \bar{\psi}(x, y) + \psi'(x, y, t) \qquad (1)$$

The mean streamfunction $\bar{\psi}(x, y)$ satisfies the mean vorticity equation when a non-barotropic source term is added. The perturbation vorticity equation may be written as

$$\left(\frac{\partial}{\partial t} + \bar{u}\frac{\partial}{\partial x} + \bar{v}\frac{\partial}{\partial y} + D_f\right)\nabla^2\psi' + \left(\frac{\partial\psi'}{\partial x}\frac{\partial}{\partial y} - \frac{\partial\psi'}{\partial y}\frac{\partial}{\partial x}\right)\left(\frac{\partial\bar{v}}{\partial x} - \frac{\partial\bar{u}}{\partial y} + \beta y\right) = 0 \qquad (2)$$

where $\bar{u} = -\partial\bar{\psi}/\partial y$, $\bar{v} = \partial\bar{\psi}/\partial x$. The linear friction term is included for computational convenience.

The flow is contained in a channel with rigid boundaries at $y = \pm D$; and the longitudinal domain is given by $x_L \leqslant x \leqslant x_R$. The mean $u$ field is given by

$$\bar{u}(x,y) = -U(x)\,\mathrm{sech}^2[y/d(x)] - U_0 \qquad (3)$$

The mean streamfunction, which is constant along the walls, takes the form

$$\bar{\psi}(x,y) = U(x)\,d(x)\,[\tanh\{y/d(x)\} + \tanh\{D/d(x)\}] + (y + D)\,U_0 - \bar{\psi}(x, -D) \qquad (4)$$

The quantity $U(x)$ can be written

$$U(x) = \left[\frac{\bar{\psi}(x,D) - 2U_0D - \bar{\psi}(x,-D)}{2d(x)}\right] \times \coth[D/d(x)] \qquad (5)$$

The $x$-variation of the jet is controlled by $d(x)$ which has the form

$$d(x) = 850\text{ km} - 350\text{ km}\cos\left(\frac{2\pi x}{\tilde{L}}\right) \quad x > x_1 \qquad (6)$$

$$= 1200\text{ km} \quad x < x_1.$$

Fig. 1 contains the $\bar{\psi}$ field and Fig. 2 contains the $\bar{u}$ field. The boundary conditions may be written

$$\psi' = 0, \text{ at } y = \pm D \qquad (7)$$

$$\psi' = A(y)\sin\omega t + B(y)\cos\omega t \text{ at } x = x_R \qquad (8)$$

$$\frac{\partial\psi'}{\partial t} = -c\frac{\partial\psi}{\partial x} \text{ at } x = x_L \qquad (9)$$

## 3. Stability properties of the parallel Jet

In this section we will discuss the local stability of the mean flow, which is obtained by assuming that the flow is parallel. The stability properties of the Bickley jet or hyperbolic-secant-squared jet have been reported extensively in the literature. The most complete discussion is given by Kuo (1973). In order to facilitate the interpretation of the numerical solutions, we determine the local growth rate and the wave structure at various points along the jet. Equation (2) is solved by the initial value technique with $\partial\bar{\psi}/\partial x = 0$ and with sinusoidal $x$-variation for $\psi'$.

Fig. 3 shows the local growth rate $n$ for the most unstable wave as a function of $x$. As expected the largest growth rate occurs at the jet maximum. The negative growth rates in the outer areas are caused by the friction. The wavelength of the most unstable wave is also shown and it follows the bahaviour of $d(x)$ [Eq. (6)].

## 4. Finite differences and a numerical procedure

The advection terms in equation (2) are approximated with the Jacobian which was developed by Arakawa (1966) to conserve mean square vorticity and kinetic energy. Euler-backward time differencing is used. The Poisson equation for the stream-function tendency is solved with the direct method developed by Sweet (1971).

The forecast equation is integrated from an initial state of $\psi' = 0$. The periodic forcing on the eastern boundary causes the interior streamfunction to grow and the integration is continued until the time variation is periodic everywhere with the forcing frequency. This frequency is varied until the value which gives the maximum perturbation amplitude is found.

## 5. Numerical Solutions

The following values are used in this experiment

$2D = 4000$ km, $x_R - x_L = 29{,}960$ km,
$\bar{u}(0,0) = -30\text{ m sec}^{-1}$, $U_0 = 0$,
$\tilde{L} = 32{,}000$ km, $\triangle x = 280$ km, $\triangle y = 125$ km.

For these parameters, the maximum response occurs for a forcing period of 3.25 days. The solution becomes fully periodic after 60 days. The $\psi'$ field at $t = 60$ days is shown in Fig. 4. It can be

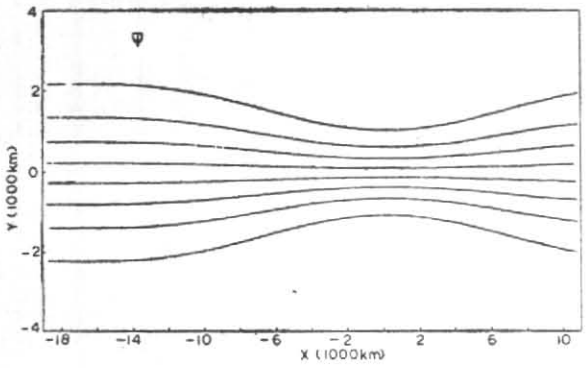


Fig. 1. The $\bar{\psi}$ field

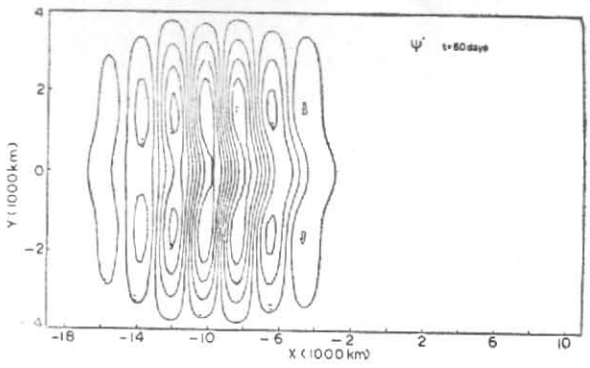


Fig. 4. The $\psi'$ field at $t=60$ days

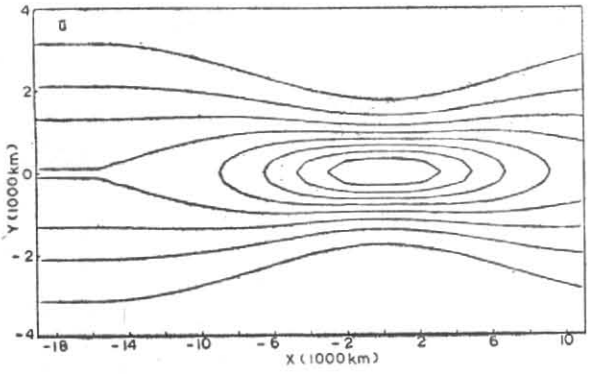


Fig. 2. The $\bar{u}$ field

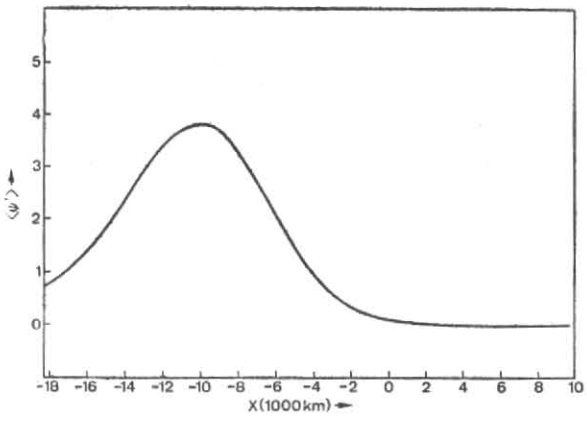


Fig. 5. The $<\psi'>$ field as a function of $x$; $<\psi'>$ is the maximum value of $\psi'$ that occurs during one period

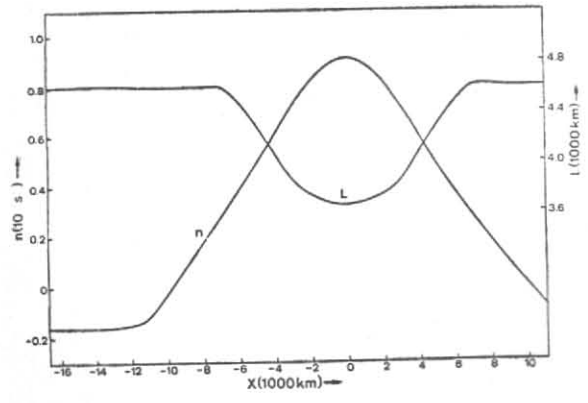


Fig. 3. The maximum growth rate, $n$, and the corresponding wavelength from the parallel flow model as a function of $x$

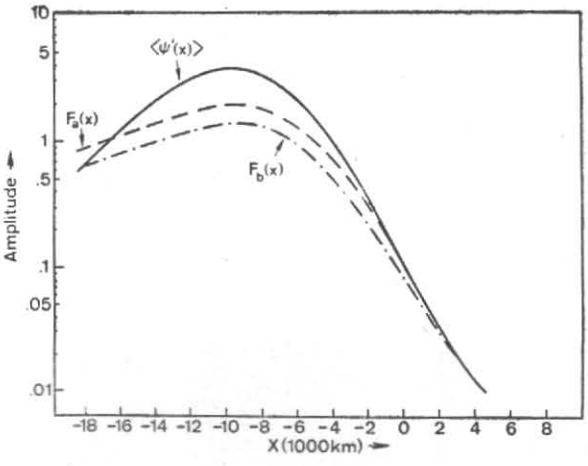


Fig. 6. Wave packet envelopes computed from the analytic (parallel flow) model $[F(x)]$ and from the complete numerical model $<\psi'>$. $F_a(x)$ is computed with $x_0 = -280$ km and $F_b(x)$ is computed with $x_0 = 4200$ km

seen that most of the waves tilt opposite to the mean wind shear, which is necessary for barotropic instability. However, near the outflow boundary the tilt is reversed; this indicates a flow of energy from the disturbance back into the mean flow. The wavelengths of the disturbances vary from 5040 km near the jet maximum to 3900 km in the outer regions.

Fig. 5 contains the wave packet envelope which is obtained when the solution is fully periodic; this envelope is evaluated at $y$=—750 km where the disturbance amplitude is large. Note that the maximum envelope amplitude occurs in the area where the local growth rate drops to zero (*see* Fig. 3). The smoothness of the fields in Figs. 4 and 5 indicate that the radiation outflow boundary condition is working properly. More results will be presented in the next Section.

## 6. Simple analytic model

In this section we develop a simple analytic model which uses the locally determined parallel flow solutions. The following equation allows for propagation and growth or decay :

$$\frac{\partial \psi'}{\partial t} + c_r(x)\frac{\partial \psi'}{\partial x} = n(x)\,\psi' \qquad (10)$$

where $c_r(x)$ is the local phase speed and $n(x)$ is the local growth rate. The quantities $c_r$ and $n$ are obtained from the parallel flow model. Clearly if $c_r$ and $n$ are independent of $x$ Eq. (10) is exact, and in general it should give a reasonable approximation to the downstream variation of $\psi'$. Now we introduce the periodic time behaviour

$$\psi' = F(x)\,e^{i\omega t} \qquad (11)$$

Substitute (11) into (10) and solve for $F$ :

$$F(x) = F(x_0)\exp\left(-i\int_{x_0}^{x}\frac{\omega}{c_r(x)}\,dx\right)\exp\left(\int_{x_0}^{x}\frac{n(x)}{c_r(x)}\,dx\right) \qquad (12)$$

Here the amplitude of $\psi'$ must be specified at $x_0$, which could be the inflow point. This formula should be applied at the latitude of maximum disturbance amplitude. In (12) the local wavelength is $\omega/c_r$ and the spatial growth rate is $n/c_r$. These are the real and imaginary parts of the wavenumber, respectively, if we were to write

$$\psi' = A\exp(ikx - i\omega t).$$

Fig. 6 compares the envelope for $\psi'$ from the complete numerical solution (Fig. 5) with the $F(x)$ given by (12) for 2 values of $x_0$. In Fig. 6 the amplitude is plotted against upstream distance. The analytic model uses the wavelengths which are measured from the complete numerical solutions. The curve for $F(x)$ can be shifted up or down by changing $x_0$, but its shape does not change. In Fig. 6 all of the curves have a maximum amplitude at $x$=—9800 km, but the simple model has a lower maximum growth rate and slower damping rates.

The lower portion of Fig. 7 contains the wavelengths which are measured from the numerical solution. The wavelength is a maximum at $x$= 1400 km which is just upwind from the place where the jet is maximum. In the upper portion of the diagram are the phase velocities, $c_r$ from the parallel flow model and $c_r$* from the complete numerical model. Here $c_r$ is computed with the use of the wavelengths shown and $c_r$* is obtained from

$$c_r^* = L\omega/2\pi \qquad (13)$$

The two phase speeds have similar behaviour although $c_r$* is shifted slightly upstream and has larger variations. In general we would expect that both the wavelength and the phase velocity would be a maximum where the mean flow is strongest, and this is generally the case although there is a slight upwind shift in the fields.

Fig. 8 contains the spatial growth rates, $m$ and $m$*, from the parallel flow model and from the complete numerical model, respectively. For the parallel flow model we have

$$m = -\,n/c_r \qquad (14)$$

This sign is chosen to represent the growth downstream. The $m$* is computed directly from the envelope. As noted in Fig. 6, $m$* has a larger maximum than $m$ and the maximum is shifted slightly downstream from the jet maximum. Both curves pass through 0 at $x$=—9800 km which is the maximum for both envelopes. However $m$* shows a much larger damping in the outflow region which can also be seen in Fig. 6. In fact the parallel flow solution damps at the rate given by the frictional coefficient divided by the phase speed.

The solutions observed in the numerical model (*see* Fig. 4) in the outflow region tilt in the same

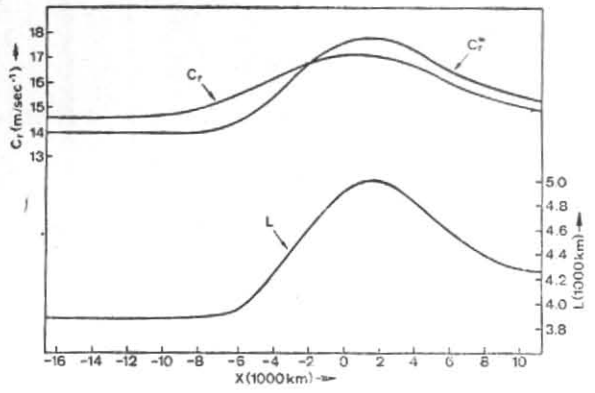


Fig. 7. The observed wavelength, $L$, and the phase velocities, $c_r$ and $c_r^*$, computed from the parallel flow model and from the complete numerical model

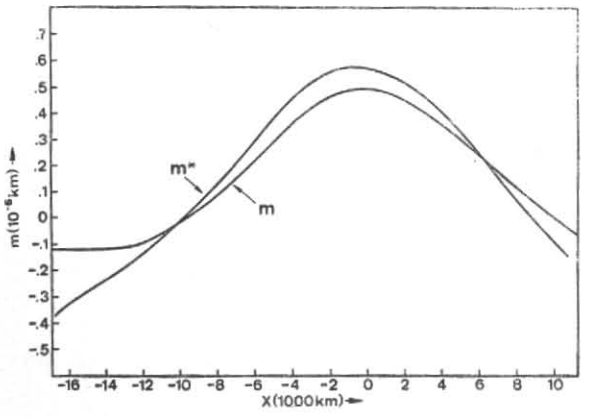


Fig. 8. Spatial growth rates, $m$ and $m^*$, computed from the parallel flow model and from the complete numerical model

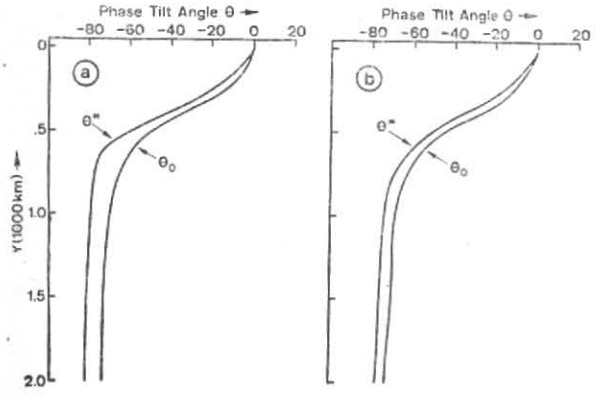


Fig. 9. Phase tilt of the waves for two longitudes : (a) $x=0$, where $\bar{u}(x, 0) = -30$ msec$^{-1}$, and (b) $x = 2800$ km, where $\bar{u}(x, 0) = -27{\cdot}3$ msec$^{-1}$, computed from the parallel flow model for the most ustable wave length and from the complete numerical model

sense as the mean wind shear which gives dynamic damping. This dynamic damping appears to be due to continuous spectrum solutions [Case (1960), Yanai and Nitta (1968)] which are not included in the normal molde solutions that are employed in the simple integral. In Fig. 8 the m* curve is skewed slightly to the left with respect to m and the jet maximum. This could be the result of the tilt structure on the wave lagging behind the value expected from the local stability conditions. This would give a smaller growth rate on the upwind side of the jet maximum and a larger growth rate on the downwind side.

The most striking feature of Fig. 8, however, is the fact that the maximum value of m* is significantly larger than the maximum value of m. Energy computations with the numerical solutions show that the most important disturbance energy production term is proportional to

$$\int \overline{u'v'} \frac{\partial \bar{u}}{\partial y} \, dy$$

This term is the only source term for the parallel flow model, and it depends on the phase tilt in the disturbance field. Fig. 9 shows the phase tilt for two values of $x$ from the numerical model and for the parallel flow model. At the jet maximum the tilt from the numerical model is significantly larger than for the tilt from parallel flow model. This is consistent with the larger growth rates for the variable jet flow. Apparently the downstream variation of the $\bar{u}$ augments the phase tilt which gives a larger growth rate.

## 7. Summary and conclusions

In this paper we have studied the behaviour of waves superimposed upon a barotropically unstable mean wind field, which varies in $x$ and $y$. This mean wind field roughly simulates the 200 mb easterly jet south of the Tibetan high during the northern hemisphere summer. A rectangular domain is employed with a time periodic boundary condition on the east and a radiation condition on the west, which simulates the propagation of small amplitude waves through the easterly jet region. The vorticity equation is solved with the use of finite differences, and when the boundary conditions are properly adjusted the waves move smoothly across the region and out the western boundary. After a certain time interval of numerical integration, the solution becomes periodic everywhere, with the frequency that is specified

on the eastern boundary. As the waves move through the domain they grow or decay spatially in reaction to the local basic flow, even though at each point the variation is purely harmonic. We have developed a simple analytical model which describes the gross features of the spatial variation. The simple model uses growth rates and phase velocities which are computed from a parallel flow model with the wavelengths taken from the full numerical model. These wavelengths increase in to a maximum near the point where the jet is most unstable, and then decrease; the phase velocity has a similar behaviour. The maximum amplitude in the numerical solution occurs downstream from the most unstable part of the jet, at the point where the growth rate in the parallel flow model becomes zero.

The maximum growth rate in the numerical model is significantly larger than the growth rate for the parallel flow model. Apparently the downstream variation of the mean wind augments the phase tilts in the waves and this causes an increased growth rate as compared with waves in a parallel flow.

The waves simulated in this study resemble the waves observed by Krishnamurti (1971), and the waves that were simulated by Colton (1973) and Chang and Pentimonti (1977). Although this study employs linear equations, it is possible to estimate the effect of the waves on the mean flow. The waves remove kinetic energy from the mean flow and most of this energy is removed on the down wind side of the jet. Clearly these synoptic scale waves will effect the amplitude and phase of the planetary waves which combine to form the easterly jet over South Asia.

*Acknowledgements*

This research was supported by the Atmospheric Research Section, National Science Foundation, under Grant DES75-10719, and by the Naval Environmental Prediction Research Facility. The numerical computations were performed by the W.R. Church Computer Centre at the Naval Postgraduate School.

*REFERENCES*


| | | |
|---|---|---|
| Arakawa, A. | 1966 | *Jour. of Com. Physics*, **1**, pp. 119-143. |
| Case, K. M. | 1960 | *Phys. Fluid*, **3**, pp. 143-157. |
| Chang, C. P. and Pentimonti, R. J. | 1978 | *Indian J. Met. Hydrol. Geophys.*, **29**, 1 & 2 pp. 205-214. |
| Colton, D. E. | 1973 | *J. atmos Sci.*, **30**, pp. 1287-1302. |
| Holton, J. R. and Colton, D. E. | 1972 | *Ibid.*, **29**, pp. 1124-1128. |
| Kanamitsu, M., Krishnamurti, T. N. and Depradine, C. | 1972 | *Ibid.*, **29**, pp. 698-706. |
| Krishnamurti, T. N. and Rogers, B. | 1970 | 200-millibar wind field June, July and August 1967, Rep. 70-2. Dep. of Met., Florida State Univ., Tallahassee. |
| Krishnamurti, T. N. | 1971 | *J. appl. Met.*, **10**, pp. 1066-1096. |
| Kuo, H. L. | 1973 | *Advan. appl. Mech.*, **13**, pp. 247-330. |
| Sweet, R. | 1971 | Subroutine POISDD, From NCAR computing facility, Boulder, 5 pp. (unpublished). |
| Yanai, M. and Nitta, T. | 1968 | *J. Met. Soc. Japan*, **46**, pp. 389-403. |